Purdue University
Purdue e-Pubs

Department of Electrical and Computer Engineering Faculty Publications

Department of Electrical and Computer Engineering

January 2008

A high sensitivity process variation sensor utilizing sub-threshold operation

Mesut Meterelliyoz

Peilin Song

Franco Stellari

Jaydeep P. Kulkarni

Kaushik Roy

Follow this and additional works at: http://docs.lib.purdue.edu/ecepubs

Meterelliyoz, Mesut; Song, Peilin; Stellari, Franco; Kulkarni, Jaydeep P.; and Roy, Kaushik, "A high sensitivity process variation sensor utilizing sub-threshold operation" (2008). *Department of Electrical and Computer Engineering Faculty Publications.* Paper 33.
http://dx.doi.org/http://dx.doi.org/10.1109/CICC.2008.4672037

This document has been made available through Purdue e-Pubs, a service of the Purdue University Libraries. Please contact epubs@purdue.edu for additional information.

A Comparison of Permanent Magnet and Wound Rotor Synchronous Machines for Portable Power Generation

Michelle Bash, *Student Member, IEEE,* Steve Pekarek, *Senior Member, IEEE,* Scott Sudhoff, *Fellow, IEEE,* Jennifer Whitmore, and Michelle Frantzen

Abstract—**Permanent magnet and wound rotor synchronous machines (PMSMs and WRSMs) are often used in diesel engine-based portable power generation systems. In these applications, there is a growing desire to improve machine efficiency in order to reduce fossil fuel requirements. In addition, there is a desire to reduce mass to improve mobility. To attempt to address these competing performance objectives, a system analyst is confronted with numerous choices, including machine type (PM or WR), converter architecture (active/passive), and control. Herein, to assist the analyst, design tools capable of performing automated multi-objective optimization of PMSMs and WRSMs connected to both active and passive rectifiers are described. The tools are then used to derive tradeoffs between mass and efficiency for a 3 kW application.**

***Index Terms*—permanent magnet synchronous machine, wound rotor synchronous machine, design, efficiency, mass, rectifier, converter**

I. Introduction

In this research, a goal was to explore the optimization of the electrical subsystem of a Man-Portable Power System (MPPS). Towards this goal, generator design programs were created for permanent magnet and wound rotor synchronous machines. The design programs were implemented within the commercial software package MATLAB. They were also configured to enable evolutionary-based multi-objective optimization using Purdue's Genetic Optimization System Engineering Toolbox (GOSET) [1]. The design codes are flexible in that they can be used to design machines (generators or motors) of arbitrary power levels and rotor speeds. This is supported by a custom material characterization station established as part of this research.

This work was supported under contract DAAB07-03-D-B009/0083 with the U.S. Army.

M. Bash, S. Pekarek, and S. Sudhoff are with the School of Electrical Engineering, Purdue University, West Lafayette, IN 47907 USA (e-mail: mbash@purdue.edu, spekarek@purdue.edu, and sudhoff@ecn.purdue.edu).

J. Whitmore and M. Frantzen are with the US Army Power and Environmental Control Engineering Support Branch, Fort Belvoir, VA 22060 USA.

As shown in Fig. 1, the MPPS consists of a diesel engine serving as the prime mover. The output shaft of the engine is connected to an electric machine that sources power electronic converters used to supply single-phase power. A multi-objective optimization was performed wherein a goal was to minimize mass and minimize loss of the electric machine. A Pareto optimal front, which shows the tradeoff between mass and loss, was obtained for machine/active rectifier and machine/passive rectifier systems.

The fronts are useful in two ways. First, for each machine, they enable one to quantify the impact that specifications on efficiency have on the mass of the machine. Second, the fronts of the respective machine/rectifiers can be compared to help select the architecture that is best suited for an application. Indeed, for the 3 kW, 3600 rpm application it appears that a permanent magnet synchronous machine has a lower mass for a given efficiency than the wound rotor synchronous machine.

II. Design Requirements and Performance Metrics

The network architecture of the MPPS studied herein is shown in Fig. 1. As shown, a 3-phase generator is used to supply power to a 407 V dc bus through a rectifier. At the output of the rectifier is a single-phase inverter that is used to source a 3 kW, 240/120 V, 60 Hz load. The diesel engine has a fixed speed (3600 rpm).

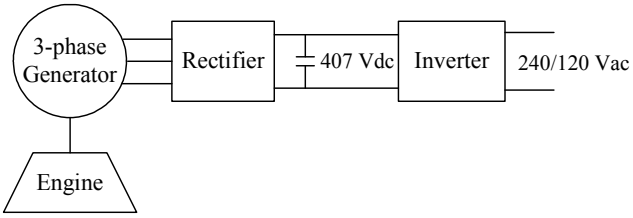

Fig. 1. Man-portable power system.

III. System I – PMSM With Active Rectifier

The first system considered for the 3 kW MPPS is a surface mounted PMSM interfaced to the dc bus with an active rectifier as shown in Fig. 2. In this system, the phase currents i_{as}, i_{bs}, and i_{cs} are regulated using a hysteresis current control so as to achieve the desired q- and d-axis currents [2]. Since

978-1-4244-5901-8/10/$26.00 ©2010 IEEE

the q-axis current is highly associated with torque and power, the q-axis current is determined by a closed loop control which attempts to regulate the dc voltage. The desired d-axis current may be determined in a number of ways including simply setting it to zero.

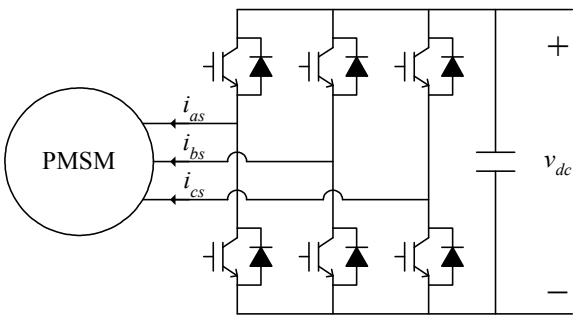

Fig. 2. System I. PMSM with active rectifier.

The machine arrangement is shown in Fig. 3. Therein, the parts of the machine are the shaft with radius r_{sh}, an inert region which is not magnetically active but which transfers torque (often accomplished with wide "spokes" in the rotor lamination) and with outer radius r_i, the rotor iron region which conducts flux circumferentially around the machine with depth d_{rb} and outer radius r_r, a permanent magnet region containing permanent magnets as well as spacers (which may be simply air) of depth d_m and outer radius r_m, an air gap of depth g, the stator slot/tooth region of inner radius r_s and thickness or depth d_s, and finally the stator backiron region of depth d_b and outer radius r_o. The length of the active part of the machine is denoted l.

A developed diagram of the permanent magnet region is shown in Fig. 4. Therein, ϕ_r denotes electrical position relative to the rotor (i.e. $P/2$ times the mechanical position measured from the q-axis of the rotor, where P is the number of poles). The quantity B_{pm} denotes the residual flux density of the permanent magnet, and χ_{pm} denotes the permanent magnet susceptibility.

The machine is assumed to have a distributed winding arrangement wherein the a-phase conductor distribution within the slot is designed to approximate the continuous distribution

$$n_{as}(\phi_{sm}) = N_p^*\left(\sin\left(\frac{P}{2}\phi_{sm}\right) - \alpha_3^*\sin\left(3\frac{P}{2}\phi_{sm}\right)\right) \quad (1)$$

In (1) N_p^* is the desired peak value of fundamental component of the conductor density; α_3^* is the relative third harmonic content used to improve slot fill. It is taken to be 0.395 herein.

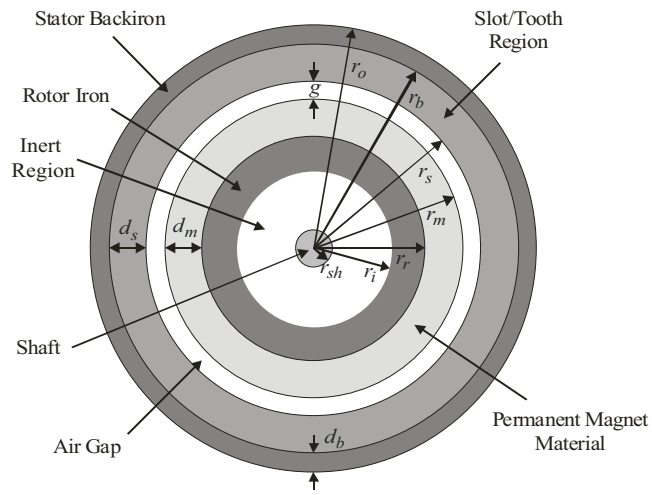

Fig. 3. PMSM Configuration.

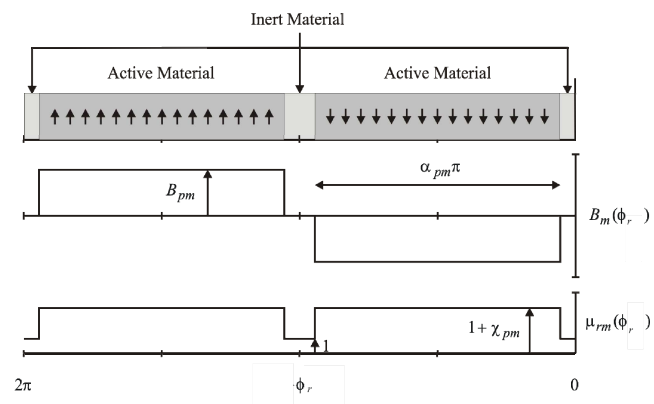

Fig. 4. Developed diagram of permanent magnet region.

The design space variables will be denoted by the vector $\boldsymbol{\theta}$. In particular, for the studies herein,

$$\boldsymbol{\theta} = \left[\alpha_{pm} \quad r_i \quad d_{rb} \quad d_m \quad g \quad d_s \quad \ldots \quad \alpha_s \quad d_b \quad l \quad N_p^* \quad i_{qs}^r \quad i_{ds}^r\right]^T \quad (2)$$

In (2), variable definitions are as follows. First, α_{pm} is the permanent magnet fraction, which is to say the fraction of the permanent magnet region filled by permanent magnet material. The variable α_s denotes the slot fraction. This may be roughly viewed as a fraction of the slot/tooth region occupied by the slot; an exact definition is given in [3]. The length of the active stack is denoted l. The quantities i_{qs}^r and i_{ds}^r denote the q- and d-axis currents [2] at the desired operating point, as defined in Section II. The remaining quantities have already been defined.

While the material choices are readily made a part of the design space (for example, see [4]), in this study they were fixed. In particular, M19 was used for the magnetic steel. The flux density limit was taken to be 1.4 T, and the density was taken to be 7402 kg/ m^3. A grade of Neodymium-Iron-Boron magnet is considered with B_{pm} of 1.1 T, χ_{pm} of 0, a minimum

field intensity of -436 kA/m, and a density of 7389 kg/m^3. It was further assumed the stator winding utilized copper. The conductivity was taken to be $58\,M\Omega^{-1}m^{-1}$ and the density to be 8900 kg/m^3.

There are several constraints on the machine design process. First, the magnitude of the flux density in all parts of the steel is limited (in this case to 1.4 T). The minimum field intensity in positively magnetized permanent magnet regions is required to exceed -436 kA/m to prevent demagnetization. The minimum airgap is required to exceed 0.002 times the rotor radius. The slot filled is required be less than 70% of the available slot area. The air gap is required to be less than 10% of the magnet depth, and the magnet depth is required to be no greater than its base circumference. The imposition of these constraints is similar to that described in [4]-[6]. Additional assumptions include a packing factor of 0.7, and end packing factor of 0.7, and an end winding offset of 1 cm. Semiconductor losses are represented as a 2 V forward drop.

The analysis upon which the evaluation of the design metrics and constraints is based is very similar to that set forth in [3]. The numerical approach to performing the optimization subject to the constraints is very similar to [4],[5].

IV. System II – PMSM With Passive Rectifier

The second system is a PMSM with a passive rectifier, as shown in Fig. 5. The arrangement of the machine is identical to that of System I.

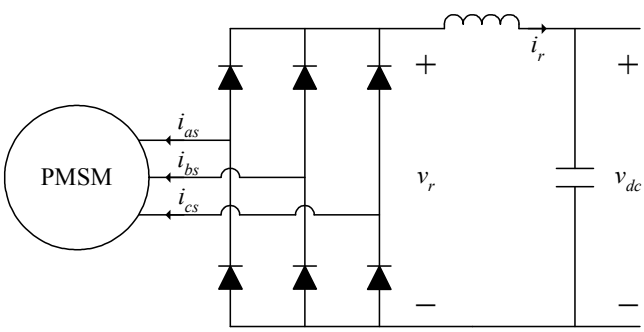

Fig. 5. System II. PMSM with passive rectifier.

Because the machine is connected into a rectifier, the q- and d-axis currents cannot be independently controlled. Thus, the design space may be expressed as

$$\boldsymbol{\theta} = \left[\alpha_{pm} \quad r_i \quad d_{rb} \quad d_m \quad g \quad d_s \quad \ldots \quad \alpha_s \quad d_b \quad l \quad N_p^* \quad i_r\right]^T \tag{3}$$

Comparing (3) to (2) it can be seen that that the rectifier current i_r replaces the q- and d-axis currents in the design space.

All design assumptions and constraints of System II are identical to those of System I, and the general methodology for optimization is also the same. However, some significant differences are present in the analysis. In essence, in System I, the currents are controlled to be sinusoidal. In System II, because of the use of an uncontrolled rectifier, the currents include significant harmonic content.

The basic approach to the analysis is thus. First, the methodology set forth in [3] is used to determine a lumped parameter model. Next, the waveform reconstruction technique set forth in [7] is used to determine the current waveforms of the machine. The methodology set forth in [3] is then modified to determine the fields as a function of rotor position with the nonsinusoidal current waveforms so that appropriate limits can be imposed and to permit calculation of flux density waveforms for the purpose of determining core losses. Publication of the details of this method will be forthcoming.

V. System III – WRSM With Active Rectifier

The third system considered is a wound-rotor synchronous machine (WRSM) interfaced to the dc bus with an active rectifier as shown in Fig. 6. In this system, the phase currents i_{as}, i_{bs}, and i_{cs} are regulated by a hysteresis current control so as to achieve the desired current waveforms [2]. In addition, the field current I_{fd} is regulated using a single-phase H-bridge circuit with hysteresis control.

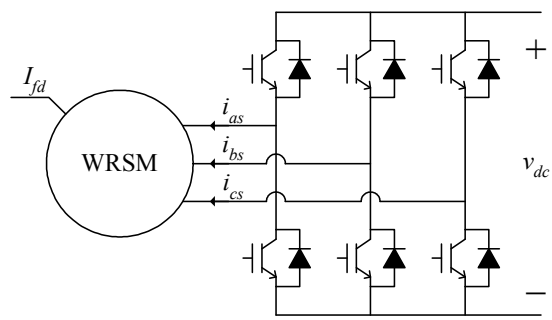

Fig. 6. System III. WRSM with active rectifier.

A basic WRSM is shown in Fig. 7 to illustrate the machine geometry. Therein, the rotor of the machine consists of the shaft with radius r_{sh}, the rotor core which conducts flux circumferentially around the machine with depth d_{rc} and outer radius r_{rc}, and the rotor teeth with depth d_{rt} and outer radius r_{rt}. The rotor teeth consist of a tooth shank connected to the rotor core with height h_{rtsh} and width w_{rtsh} and a tooth tip with width w_{rtt} and an outside edge height of h_{rtt}. The number of rotor teeth is equivalent to the number of poles. The airgap has a uniform depth between stator and rotor teeth of g. The stator of the machine consists of the stator teeth with depth d_{st} and inner radius r_{si}, the stator slots with a width of w_{ss} at the airgap, and the stator back iron of depth d_b and outer radius r_o. The stator can have any integer number of slots per pole per phase. The length of the active part of the machine is denoted l.

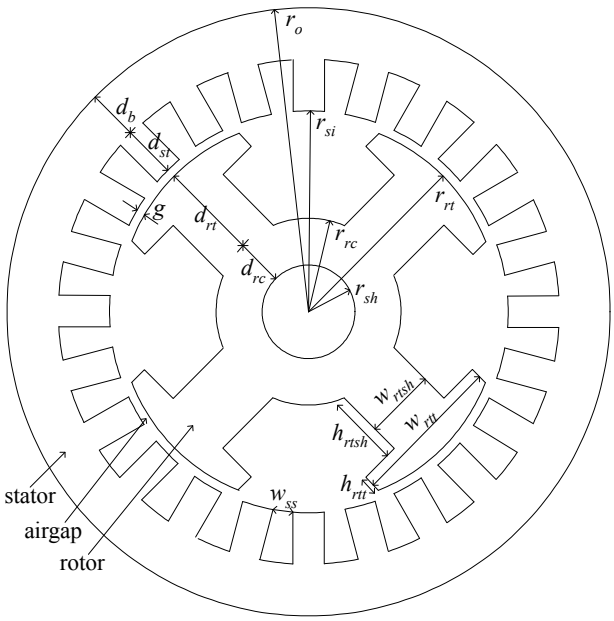

Fig. 7. Example WRSM configuration.

The WRSM is modeled using a flexible and efficient magnetic equivalent circuit (MEC) technique. A portion of the equivalent circuit for an arbitrary geometry is shown in Fig. 8 in developed diagram form. The circuit configuration changes with the rotor position θ_r, which is defined in Fig. 8 as the relative position of the q-axis with respect to the as-axis. The flux paths in the stator, rotor, and airgap are represented by equivalent reluctance elements (shown in Fig. 8 using the resistance symbol), and the currents in the machine are represented by equivalent sources of magnetomotive force (mmf). The basic concept of the MEC model is to calculate the flux in the machine by solving a nonlinear system of circuit equations. Winding current is an input to the model, winding flux is an output, and the system is nonlinear due to magnetic saturation. Further details about the MEC model are provided in [8].

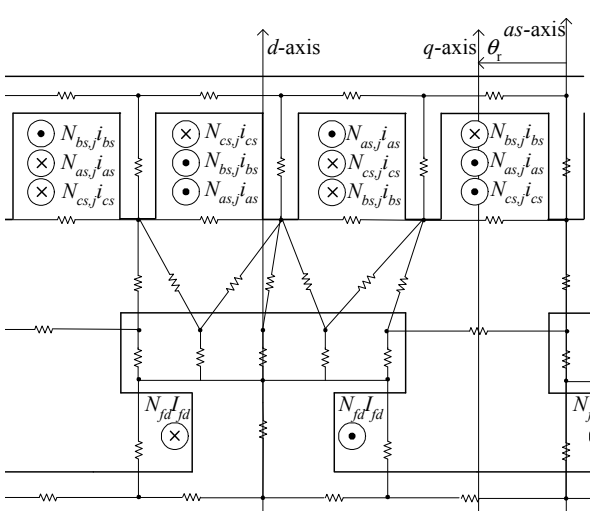

Fig. 8. Example WRSM MEC, including phase and field windings.

The phase and field windings are also depicted in Fig. 8. As shown, a discrete representation of the phase windings is used wherein the turns variables $N_{as,j}$, $N_{bs,j}$, and $N_{cs,j}$ indicate the number of a-, b-, and c-phase turns in the j-th stator slot. The turns variables must be selected to create balanced and symmetric windings. In the design studies herein, there is only one non-zero turn variable associated with each slot, which results in a concentrated winding. The field winding is bobbin-wound around the rotor tooth shank, and the term N_{fd} indicates the number of field turns.

The design space variables for the studies relating to system III are given by,

$$\begin{aligned}\boldsymbol{\theta} = \big[& r_{sh} \quad d_{rc} \quad l \quad d_{rt} \quad g \quad d_{st} \quad d_b \quad fw_{ss} \quad \cdots \\ & fh_{rtt} \quad fw_{rtt} \quad fw_{rtsh} \quad N_s \quad I_s \quad \beta \quad N_{fd} \quad I_{fd} \big]^T\end{aligned} \tag{4}$$

In (4), the first seven variables relate to the machine geometry, and they were defined earlier when discussing Fig. 7. The next 4 variables are denoted with an f preceding a previously discussed geometry variable. These 4 variables define the geometric value as a fraction of some other machine geometry. For instance, with the inner stator radius and the number of teeth known, fw_{ss} defines the width of the stator slot as a fraction of the total width of one slot plus one tooth. The variable N_s denotes the number of turns in the concentrated phase windings. The variable I_s defines the rms phase current, and β defines the phase angle of the stator currents. The resulting phase currents are given by,

$$\begin{bmatrix} i_{\mathrm{as}} \\ i_{\mathrm{bs}} \\ i_{\mathrm{cs}} \end{bmatrix} = \sqrt{2} I_{\mathrm{s}} \begin{bmatrix} \cos(\theta_{\mathrm{r}} + \beta) \\ \cos(\theta_{\mathrm{r}} + \beta - 2\pi/3) \\ \cos(\theta_{\mathrm{r}} + \beta + 2\pi/3) \end{bmatrix} \tag{5}$$

The variable N_{fd} denotes the number of field turns, and I_{fd} is the field current.

As discussed in Section III, the choice of material can be readily included in the design space; however, for the studies herein, the material type was fixed. As in Systems I and II, M19 was used for the magnetic steel, and copper was used for the stator and field windings.

In order to meet general WRSM design specifications, several constraints are placed on the machine performance. Specifically, the output power of the machine must be greater than the required output power. In addition, for thermal reasons, a limit is placed on the maximum current density in the stator and rotor. Both the stator and rotor current densities are calculated as the ratio of current to conductor area, where the conductor area is determined assuming a maximum slot fill with a packing factor of 0.7 in the stator and 0.8 in the rotor. There is also a constraint placed on the dc-link voltage required to produce the phase currents. The constraint ensures that the required voltage is less than or equal to the intended dc-link voltage.

In addition to meeting design specifications, several

constraints are needed to ensure that the model is operating correctly. The first constraint ensures that the geometry of the machine is physically realizable (all values are non-negative). The second constraint limits the maximum value of flux density in the machine since the MEC has not been structured to evaluate machines operating at exceedingly high levels of saturation. A value of 1.64 T was selected for M19 since the material characterization yielded a relative permeability of 200 at that operating point. Finally, a constraint is included to ensure that the nonlinear WRSM model converges to a solution. All constraints are implemented using a similar approach to the one in [3].

VI. System IV – WRSM With Passive Rectifier

The fourth system is a WRSM with a passive rectifier, as shown in Fig. 9. The dc bus voltage v_{dc} is assumed to be a user-specified constant value. The configuration of the machine is identical to that of System III.

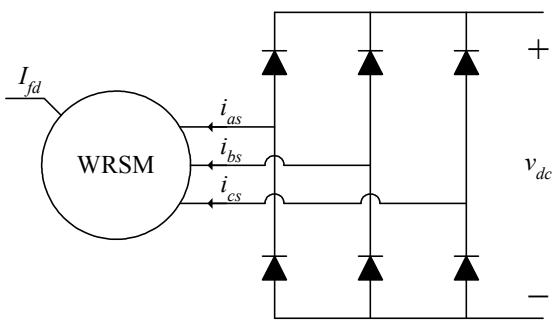

Fig. 9. System IV. WRSM with passive rectifier.

In connecting to a passive instead of an active rectifier, the phase currents can no longer be controlled. Instead, the phase currents are dependent upon the dynamics of the machine and the rectifier. As a result, the structure of the WRSM model is significantly different. To describe briefly, the MEC system is restructured to have flux linkage as an input and phase current and flux as outputs. In addition, a model of the passive rectifier is used to determine the machine voltages based upon the phase currents. A numerical integration routine is applied to solve the machine differential equations with phase flux linkage as the state variable. In the dynamic model, it is assumed that the field current is still controlled to be a constant value in order to avoid the slow rotor time constant.

The design space for System IV is expressed as

$$\boldsymbol{\theta} = \left[r_{sh} \quad d_{rc} \quad l \quad d_{rt} \quad g \quad d_{st} \quad d_b \quad fw_{ss} \quad \cdots \quad fh_{rtt} \quad fw_{rtt} \quad fw_{rtsh} \quad N_s \quad N_{fd} \quad I_{fd} \right]^T \tag{6}$$

where the variables related to the phase currents have been removed. All design assumptions and constraints of System III also apply to System IV with one exception. The constraint on the calculated dc bus voltage is no longer needed for System IV since the bus voltage is pre-defined.

VII. Comparison of Systems I-IV

The design programs described in Sections III-VI were applied herein to explore the optimization of a 3 kW MPPS with specifications given in Section II. The objectives of the design were to minimize the machine mass and minimize the power loss. The resulting Pareto fronts for Systems I-IV are shown in Fig. 10. A machine topology of 4 poles and 2 stator slots per pole per phase was used in all four design studies.

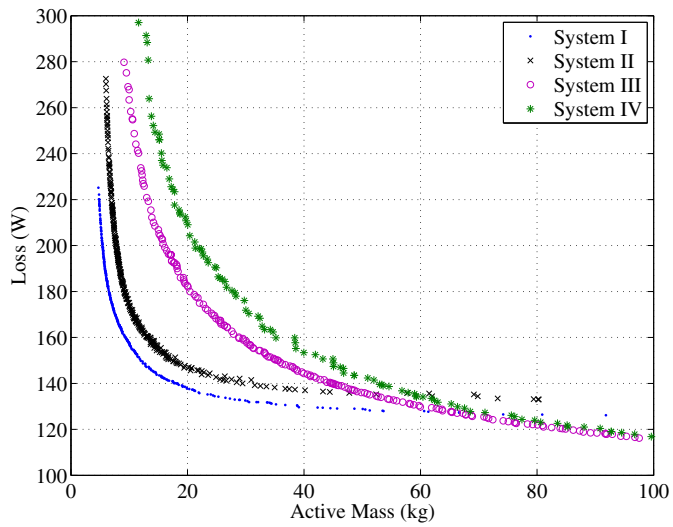

Fig. 10. Pareto fronts for Systems I-IV.

The Pareto fronts presented in Fig. 10 are useful to a designer in several ways. First, considering the fronts individually, a designer can readily evaluate the mass versus loss tradeoffs for each system. As a result, the impact of imposing efficiency requirements (or weight requirements) is readily quantified. Second, the tradeoffs associated with an active versus passive rectifier can be readily evaluated. For both the PMSM and WRSM, the active rectifier outperforms the passive rectifier; however, depending on the exact difference in performance, the passive rectifier may be more attractive since it requires less control effort. With the Pareto fronts in hand, a designer can readily choose the most appropriate rectifier architecture for the MPPS application. Finally, the fronts shown in Fig. 10 allow one to readily compare a PMSM- and WRSM-based system. For the application considered herein where portability is a significant factor, one can see that a PMSM provides the same efficiency as a WRSM at a fraction of the mass.

VIII. Conclusion

In this paper, design programs have been presented for PMSMs and WRSMs connected to active and passive rectifiers. The design programs consider a large number of design variables and multiple optimization objectives. In addition, the programs are flexible allowing the user to explore a wide range of machine/rectifier applications. Herein, the design programs were applied to explore the optimization of the electric machine/rectifier component of a MPPS. The Pareto fronts obtained from the program enable the designer to

consider various design tradeoffs in an effective and thorough manner. Specifically, the user can evaluate tradeoffs in mass versus loss for each individual system and between the different system architectures.

REFERENCES

[1] S.D. Sudhoff, Y. Lee "Energy Systems Analysis Consortium (ESAC) Genetic Optimization System Engineering Tool (GOSET) Version 1.05 Manual," School of Electrical and Computer Engr., Purdue Univ., http://cobweb.ecn.purdue.edu/~sudhoff/Software%20Distribution/index.html, 2003.

[2] P.C. Krause, O. Wasynczuk, S.D. Sudhoff, *Analysis of Electric Machinery and Drive Systems, 2nd Edition,* IEEE-Press, Piscataway, NJ through Wiley-Interscience. 2002.

[3] B.N. Cassimere, S.D. Sudhoff, "Analytical Design Model for Surface Mounted Permanent Magnet Synchronous Machines", *IEEE Transactions on Energy Conversion,* vol. 24, no. 2, pp. 338-346, June 2009.

[4] B.N. Cassimere, S.D. Sudhoff, "Population Based Design of Permanent Magnet Synchronous Machines," *IEEE Transactions on Energy Conversion,* vol. 24, no. 2, pp. 347-357, June 2009.

[5] B. Cassimere, R. Chan, J. Cale, A. Cramer, S. Sudhoff, "Evolutionary Design of Electromagnetic and Electromechanical Devices," *IEEE Electric Ship Technologies Symposium*, Arlington, VA, May 21-23, 2007.

[6] S.D. Sudhoff, J. Cale, B. Cassimere, M. Swinney, "Genetic Algorithm Based Design of a Permanent Magnet Synchronous Machine," *2005 International Electric Machines and Drives Conference*, San Antonio, Texas, May 15-18, 2005.

[7] S.D. Sudhoff, "Waveform Reconstruction in the Average-Value Modeling of Line-Commutated Converter – Synchronous Machine Systems," *IEEE Transactions on Energy Conversion*, Vol. 8, No. 3, pp. 404-410, September 1993.

[8] M. Bash, J. Williams, and S. Pekarek, "Incorporating motion in mesh-based magnetic equivalent circuits," *IEEE Transactions on Energy Conversion*, accepted for future publication.